Ground-State Proton-Transfer Tautomer of the Salicylate Anion

D. M. Friedrich,* Z. Wang, and A. G. Joly

Environmental and Molecular Science Laboratory, Pacific Northwest National Laboratory, Richland, Washington 99352

K. A. Peterson†

Department of Chemistry, Washington State University, Richland, Washington 99352

P. R. Callis

Department of Chemistry, Montana State University, Bozeman, Montana 59717

Received: February 3, 1999; In Final Form: July 30, 1999

Solutions of sodium salicylate in anhydrous polar solvents exhibit a weak, temperature-dependent absorption band ($\lambda_{max} \approx 325$ nm) lying in the Stokes gap between the main absorption (296 nm) and the fluorescence band (396 nm, acetonitrile). This weak, longer wavelength absorption band is hardly observable in aqueous solution, but its intensity increases with temperature and increases with polarity in anhydrous organic solvents in the order of ethanol < acetonitrile < dimethyl sulfoxide at room temperature. After correction for solvent thermal contraction, the temperature-dependent absorption spectrum of salicylate in acetonitrile solutions reveals a clear isosbestic point ($\epsilon_{310} = 2000$ M^{-1} cm^{-1}) characteristic of an equilibrium between two salicylate species with band-maximum extinction coefficients of $\epsilon_{325} = 3400$ M^{-1} cm^{-1} and $\epsilon_{296} = 3586$ M^{-1} cm^{-1}. In acetonitrile at room temperature (298 K) the concentration equilibrium constant (minor/major) for the interconversion reaction between the two species is $K_{298} = 0.11$, with $\Delta H = 1.6$ kcal mol^{-1} and $\Delta S = 0.97$ cal·mol^{-1} K^{-1}. The fluorescence lifetime (4.8 ns in acetonitrile) and the shape of the fluorescence spectrum are independent of excitation wavelength. The fluorescence quantum yield for excitation in the long-wavelength shoulder (340 nm) is approximately 60% larger than the yield for excitation in the main band at 296 nm ($\varphi_{340} = 0.29$, $\varphi_{296} = 0.18$) in acetonitrile at room temperature. These results are consistent with assignment of the shoulder band to the proton-transfer tautomer of the salicylate anion. Electronic structure calculations support assignment of the 325 nm absorption band to the ground-state tautomer (phenoxide anion form) of the salicylate anion. Absorption transition moments for both the normal and tautomer forms are parallel to the emission transition moment, are electronically allowed, and are consistent with ^1L_b assignment for both absorbing and emitting transitions. The static dipole moments are in the order of $\mu(N^*) \geq \mu(N) > \mu(T^*) > \mu(T)$ for the normal (N) and tautomer (T) ground and electronic excited states.

Introduction

Proton transfer between tautomers in excited electronic singlet states has been well established for several families of organic compounds with the potential for intramolecular, intermolecular, or solvent-bridged hydrogen bonding between a proton donor (such as a phenolic hydroxyl group) and a proton acceptor (such as a carbonyl oxygen).[1,2] The photocycle for intramolecular hydrogen-bonded (IHB) systems ($N + h\nu_e \rightarrow N^* \rightarrow T^* \rightarrow T + h\nu_f \rightarrow N$)[3] is supposed to proceed on the pathway of excitation ($h\nu_e$) of the stable "normal" IHB conformation (N), followed by excited-state intramolecular proton transfer (ESIPT) to the proton-transfer tautomer (T*). Emission from T* ($h\nu_f$) has a characteristically large Stokes gap (>8000 cm^{-1}). The nature of the potential energy surface of the ground state at the equilibrium geometry of the excited state of proton-transfer tautomers remains an active area of experimental and theoretical study.[4,5] While the ground-state tautomers (T) of ESIPT systems are often reasonably assumed to be unstable (i.e., with no ground-state local minimum at the equilibrium nuclear configuration of the excited-state T*), nevertheless a few stable ground-state tautomers of ESIPT systems have been observed or inferred.[6−14] It is evident that the polarity and H-bonding strength of solvents affect the stabilization of ground-state tautomers. Recently[15,16] Bisht et al. interpreted the pressure-induced increase of the emission intensity of salicylic acid in nonpolar methylcyclohexane as partly due to increased formation of the ground-state tautomer with pressure. They deduced a partial molar volume change of −4.3 cm^3/mol for N → T tautomerization. We discuss here the evidence for existence of a metastable ground-state proton-transfer tautomer (T) of the salicylate anion in equilibrium with the normal form (N) in anhydrous polar solvents.

Dual fluorescence of salicylate esters and derivatives has formed the basis for extensive experimental and theoretical tests of the ESIPT hypothesis originally proposed by Weller for methyl salicylate.[17] It is now accepted that two fluorescing methyl salicylate rotamers exist in equilibrium, each with a

* To whom correspondence should be addressed. Current address: Optical Coating Laboratory, Inc., 2789 Northpoint Parkway, Santa Rosa, CA 95407-7397. E-mail: dfriedrich@ocli.com.

† Also the Environmental and Molecular Science Laboratory, Pacific Northwest National Laboratory, Richland, WA 99352.

10.1021/jp990405+ CCC: $18.00
Published on Web 11/10/1999

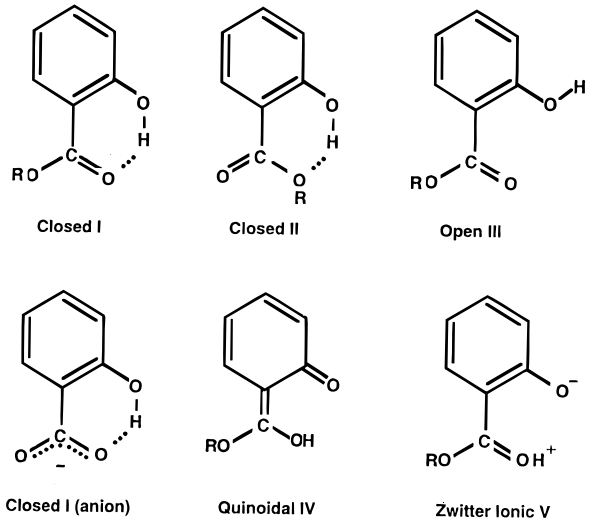

Figure 1. Structures of salicylate esters.

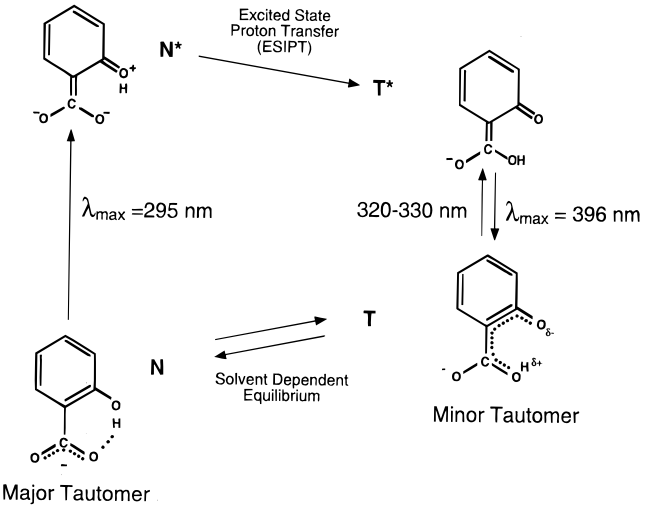

Figure 2. Proposed dominant electronic resonance structures of the salicylate anion photocycle.

distinct excitation spectrum and fluorescence (structures I and II in Figure 1).[18−22] A third, open form (III) also can be trapped and shows only short-wavelength emission from N*.[21,22] ESIPT between the phenolic −OH and the carbonyl oxygen of the ortho carboxylate group is now recognized as the source of long-wavelength fluorescence in rotamer (I). Rotamer (II) shows only short wavelength ("normal" or N*) fluorescence characteristic of a phenolic species. The rapid rise time of the long-wavelength emission in methyl salicylate indicates that the ESIPT rate is faster than 10^{11} s^{-1}.[23] It is now believed there is no significant equilibrium between N* and T* and that ESIPT is barrierless in many salicylate derivatives.[24] The structure of the excited-state tautomer is a resonance hybrid between the quinoidal form (IV) and the phenoxide tautomeric form (V) which is zwitterionic in the neutral derivatives. Electron redistribution in the excited-state isomers and the shape of the excited potential energy surface (single or double minimum) remain active areas of study. On the excited-state potential energy surface the proton moves from the hydroxyl oxygen atom to an ortho carboxyl or aldehyde oxygen in response to electronic charge transfer in the excited state from the donor (increasing the acidity of the proton donor) to the aromatic ring and acceptor system (increasing its basicity).[25−39] Direct evidence for the coupling of excited-state proton transfer with excited-state electron transfer has been reported for salicylic acid,[40] imidazopyridines,[41] aminosalicylates[42,43] and amine-substituted flavones.[44−46] The nature of the ground state at the ESIPT equilibrium nuclear configuration (i.e., at the geometry of T*) also has been an open question of whether T is a metastable intermediate (represented by a resonance form such as IV or V) in equilibrium with the normal (N) phenolic ground state (closed form I) or whether the proton undergoes rapid, barrierless back-transfer on the ground-state surface following fluorescence.[47−49] For example, equilibria in the ground and excited states are controlling parameters for proposed lasing action of ESIPT compounds.[13,14,50−52]

At room temperature the predominant ground-state isomer of salicylate anion possesses an intramolecular hydrogen bond between the phenol and carboxylate groups (N in Figure 2). Calculations and experiments agree that the H-bonded phenol and carboxylate groups lie in the plane of the phenyl ring.[4,12,53,54] FTIR spectra show that the closed IHB structures I and II of salicylate monoanion are identical since both carboxyl oxygens are equivalent.[55,56] Because of the delocalized negative charge and the coplanarity of the phenyl-ring and carboxylate groups, the salicylate phenol group forms a strong intramolecular hydrogen bond with the carboxyl group in all solvents. The lowest energy absorption of the first excited singlet state of aqueous salicylate anion lies in the quartz UV (296 nm) as expected of an ortho disubstituted benzene derivative. Despite the low symmetry of salicylate, the Franck−Condon accessible lowest excited singlet state can be roughly correlated with the ^1L_b state of substituted benzene compounds.[57,58] In the excitation sufficient electronic charge is transferred from the hydroxyl oxygen to the phenyl ring to create a potential gradient leading to proton transfer. What distinguishes the fluorescence of salicylate anion, its esters, and its derivatives from that of many other disubstituted phenyl compounds is its unusually long wavelength (415 nm for the aqueous anion). While the gap between excitation and fluorescence maxima (Stokes gap) is typically 4000−6000 cm^{-1} in disubstituted benzenes, the Stokes gap of aqueous salicylate anion is 9700 cm^{-1}. Such large Stokes gaps are indicative of a large geometry change and subsequent relaxation in the excited electronic state, such as ESIPT in aromatic compounds that contain a strong IHB.[18,59−61] Unlike many methyl salicylate and related neutral compounds which give both short (N*) and long (T*) wavelength emission, the salicylate anion only shows the Stokes-shifted blue emission (T*) even in such a strong polar protic solvent as water. The lack of near UV emission (N*) is evidence that the non-IHB open forms and solvent disruption of IHB are both absent in the anion. Salicylate anion has a higher fluorescent quantum yield than the other neutral salicylate derivatives. These properties make salicylate a useful spectroscopic probe in scintillation counting, biochemistry, pharmacology, and metal ion complexation in natural waters.[62−65]

A readily available published spectrum of sodium salicylate in ethanol[59] documents its unusual photophysics. The fluorescence maximum (403 nm) is separated from the absorption maximum (296 nm) by approximately 8970 cm^{-1}. Such a large gap between absorption and emission bands must represent significant nuclear rearrangement in the excited state and is taken as evidence for ESIPT in the anion. Inspection of the Berlman absorption spectrum for ethanolic sodium salicylate[59] reveals a wide, long-wavelength tail (330−350 nm) that is not characteristic of $S_1 \leftarrow S_0$ absorption band shapes of the substituted benzenes. In this paper we show that the long-wavelength absorption tail is due to a salicylate isomer (the tautomer T) that is stabilized in anhydrous nonprotic polar solvents and that

this isomer has the same fluorescence band shape as that created by excitation of the stable ground-state isomer (N). The extinction coefficient, fluorescence anisotropy, and fluorescence decay time constant for the less stable isomer are nearly identical to those of the stable form. The relative amount of the isomer form varies with solvent protic character and with temperature. Assignment of this isomer to the ground-state proton-transferred tautomer (phenoxide anion form) of the salicylate monoanion is consistent with the observed spectroscopic, thermal, and chemical properties of the 325 nm absorption band. We will show that the conversion between the short- and long-wavelength absorption bands is intramolecular and is not due to dimerization, protonation (forming salicylic acid), or hydroxyl deprotonation (forming salicylate dianion). This optical spectroscopic identification of the ground-state phenoxide tautomer of the salicylate monoanion opens the possibility to study the complete ESIPT photocycle by direct excitation of both tautomers.

Experimental Section

Sodium salicylate, reagent grade, was purchased from Mallinckrodt Chemical Co. Salicylic acid, reagent grade, was purchased from Aldrich. Anhydrous dimethyl sulfoxide, spectrophotometric grade ethanol, and acetonitrile were purchased from Aldrich in septum-capped bottles. Sodium hydroxide, perchloric acid, sodium perchlorate, acetic acid, triethylamine, and deuterium oxide were purchased from Aldrich. All chemicals were used as received without further purification. Solvent transfers from the original bottles were performed under the protection of dried N_2 with Teflon syringes. Solutions of sodium salicylate, salicylic acid, acetic acid, and triethylamine in organic solvents were prepared by weighing the compounds and immediately transferring them into glass solvent tubes that were sealed with Teflon-lined caps. Tubes were opened only when the solution was transferred to the spectroscopic cell. All spectroscopic measurements were carried out in UV quartz cells with matched Teflon caps and further sealed with Parafilm.

The aqueous solutions were prepared using spectroscopic grade water from a Millipore reversed osmosis and ion exchange system, with ultraviolet sterilization of the finished water. Care was taken to avoid long periods of water−plastic contact to eliminate contamination of the water with residual phthalates often associated with plastic tubing and vessels. The pH's of the aqueous solutions were adjusted using solutions of analytical grade sodium hydroxide or perchloric acid and measured on an Orion Model 720A pH meter equipped with an Orion microelectrode.

Absorption spectra were measured on a Cary 3 spectrophotometer. Fluorescence and excitation spectra were recorded using a SPEX Fluorolog II fluorometer equipped with two double monochromators (SPEX1680), a 450 W xenon lamp, and a cooled photomultiplier. Excitation spectra were corrected for spectral variation of the excitation light intensity. The spectral response of the emission detection system was nearly constant across the emission wavelength range (350−450 nm), and therefore the reported emission spectra were not corrected for spectral response.

For experiments at temperatures lower than room temperature, an atmospheric pressure, flow-through cryogenic work station equipped with four pairs of Suprasil quartz windows was used (Cryo-Industries of American RC 152). In this apparatus liquid nitrogen is evaporated and temperature controlled by an internal heater before passing over a 3 or 5 mm square quartz tube containing the liquid sample. Gas-phase cooling of the sample allows homogeneous cooling of an unsealed sample at ambient pressure and avoids interference of the spectroscopic measurements from turbulence and gas bubble formation in liquid nitrogen. The cell temperature was controlled by a Lakeshore 330 autotuning temperature controller (±0.01 °C). To correct for the solvent contraction at lowered temperatures in the temperature-dependent absorption spectra, it was assumed that the sum of the oscillator strengths of the normal species and tautomer is constant in the entire temperature range studied on the basis of the similar structures of the two species and, more importantly, the fact that the normal species is always predominant in the absorption spectra at all the temperatures. Thus, solvent contraction is compensated by normalizing the areas under the absorption curves of the spectra at lowered temperatures to the area under the absorption curve at room temperature.

Fluorescence lifetime measurements were carried out on a time-correlated single-photon-counting (TCSPC) apparatus constructed in our laboratory.[66] Laser excitation was provided with the frequency-doubled output of a cavity-dumped Coherent 702 dye laser operating between 580 and 610 nm (290−305 nm, frequency-doubled) or a Coherent Satori 774 dye laser operating between 620 and 683 nm (310−341 nm, frequency-doubled). The dye lasers were pumped by the second harmonic of a mode-locked Coherent Antares Nd:YAG laser operating at 76 MHz. The sample fluorescence emission was collected with a pair of parabolic mirrors and focused onto an American Holographic double monochromator. The dispersed light was detected by a microchannel plate photomultiplier. The laser pulse width was less than 3 ps, and the measured instrument response was typically between 20 and 30 ps fwhm. For each lifetime measurement, the decay curve has a minimum of 10^4 counts in the peak intensity channel.

The steady-state fluorescence anisotropy (R) of a sample is defined as the difference between the vertical (I_v) and horizontal (I_h) polarization components of emission intensity, divided by the total emission intensity, $R = [I_v - I_h]/[I_v + 2I_h]$, where the polarization components I_v and I_h have been corrected for instrumental polarization bias in the standard ways using both horizontal excitation of I_v and I_h in the frozen samples and also a room-temperature diluted cyclohexane solution of anthracene.[67−70] For the steady-state anisotropy measurements in the fluorometer, Glan-Thompson polarizers were placed in both the excitation and emission light paths. A polarization scrambler was placed immediately behind the polarizer on the emission side to ensure undiscriminated response of the monochromator and optical system to emitted light of either polarization.

The time-resolved fluorescence anisotropy, $R(t)$, was determined using measured time-dependent intensities of the vertical and horizontal fluorescence polarizations, $R(t) = R_0 \exp(-t/\tau_r)$.[71] Time-resolved fluorescence anisotropy was measured on a Hamamatsu 5680 streak camera equipped with M5675 synchroscan and M5678 synchroblanking units. Laser excitation was provided by the frequency-doubled dye laser system described above. The system response function varied from 3 to 15 ps, depending on thermal drift and jitter in the timing of the laser pulses. To measure the vertical and horizontal polarization components of fluorescence intensity, $I_v(t)$ and $I_h(t)$, using the streak camera, the polarization analyzer was rotated manually between vertical (v) and horizontal (h), collecting 750 laser pulses in each orientation. The analyzed decay curves $I_v(t)$ and $I_h(t)$ are the result of at least 10

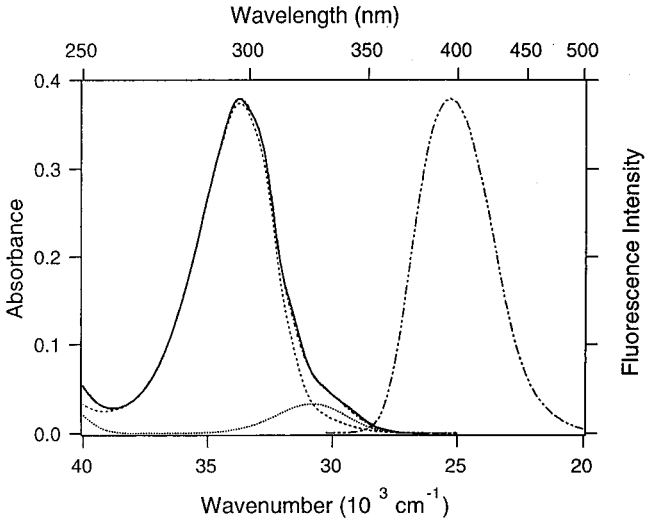

Figure 3. Absorption and fluorescence spectra of sodium salicylate in dry acetonitrile showing deconvolution of the two absorption bands under the absorption spectrum.

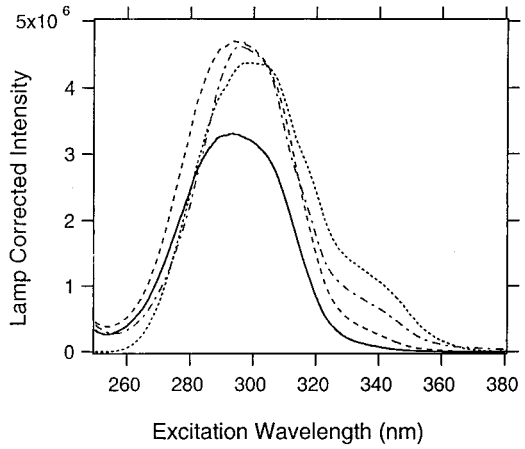

Figure 4. Excitation spectrum of sodium salicylate in various solvents, corrected for spectral variation of excitation light intensity. Comparison with the absorption spectrum (Figure 3) shows qualitatively that quantum yield ϕ_{340} is higher than ϕ_{296}.

accumulations (i.e., >7500 laser pulses) with at least 10^4 counts in the peak time channel.

Results and Discussion

Absorption and fluorescence spectra of sodium salicylate in dry acetonitrile at room temperature (28 °C) are shown in Figure 3. The extinction coefficient (molar absorptivity) of sodium salicylate in acetonitrile was determined by a Beer's law plot to be 3586 ± 40 M^{-1} cm^{-1} at the band maximum (296 nm). The weak long-wavelength shoulder seen in the absorption spectrum is enhanced by a factor of approximately 2 in the intensity-corrected emission excitation spectrum (Figure 4). The shape of the fluorescence band is independent of excitation wavelength over the range investigated (280−360 nm). Relative to the main excitation band at 296 nm, the intensity of the long-wavelength shoulder band increases with solvent polarity but decreases with increasing solvent protic (hydroxyl) content. For example, the effect of increasing mole fraction of water on the absorption spectrum in salicylate/acetonitrile/water solutions is shown in Figure 5. An isosbestic point is observed at 309.5 nm, and the shoulder band is very weak at the highest water concentration (2.4 M H_2O). In a completely aqueous solution of salicylate (no acetonitrile) the shoulder is hardly

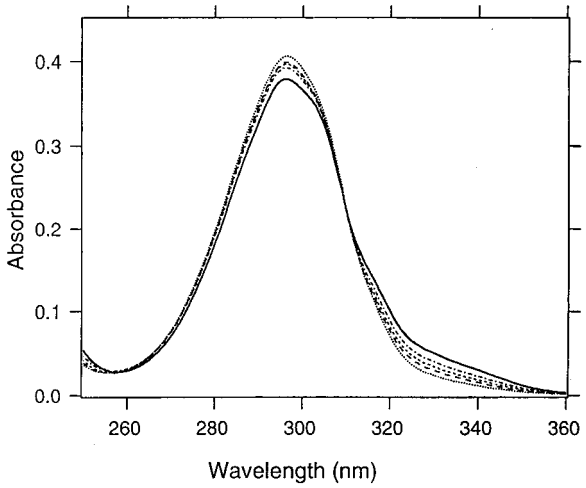

Figure 5. Effect of adding water on the absorption spectrum of sodium salicylate in acetonitrile. The ratio of tautomer to normal absorbance decreases with increasing concentration of water. Note the isosbestic point at 310 nm.

observed. An isosbestic point at 309.5 nm also is seen in the temperature-dependent absorption spectra which have been corrected for solvent contraction (Figure 6). These isosbestic points are taken as evidence of an equilibrium between two ground-state isomers of the salicylate anion. The major isomer is responsible for the main absorption band at 296 nm, while the absorption band of the minor isomer lies under the main band, in the longer wavelength shoulder (320−340 nm). We assign the main absorption band to the normal form isomer (N) and the shoulder band to its proton-transfer tautomer (T). The following results and discussion support this assignment.

Salicylate anion is in equilibrium with its protonated form at low pH (salicylic acid, aqueous pK_a = 2.95) and with its doubly depronated form at high pH (salicylate dianion, aqueous pK_a = 13.4). To investigate the possibility that the shoulder band may be due to either salicylic acid or the dianion, 10^{-4} M solutions of sodium salicylate in acetonitrile were separately titrated with acetic acid and with triethylamine up to 1.5×10^{-3} M in acid or base. In both titrations there was no observable change in the ratio of absorbance of the two bands, A_{300}/A_{325}. The finalconcentration of acid and base in these titrations represents an excess of 15 over the salicylate concentration. Formation of dimers or higher oligomers can cause absorption bands to be polarity and temperature dependent. The ratio of fluorescence excitation intensities of the deconvoluted bands (I_{300}/I_{325} = 5.3 ± 0.3) did not vary systematically over the concentration range 10^{-7}−10^{-4} M. These results give confidence that only monomer salicylate is responsible for the spectra observed in the acetonitrile solutions of this study.

To estimate the relative concentration of the two isomers, the absorption spectra were decomposed into two component curves using the following procedure. The more intense 296 nm component was first approximated by using the absorption spectrum of salicylate in aqueous acetonitrile solution (2.4 M H_2O in CH_3CN), which is nearly free of the longer wavelength shoulder. The main band at 296 nm has similar structure and shape in both dry and wet acetonitrile. The spectrum of salicylate in wet acetonitrile was then scaled to give a good fit to the spectrum of salicylate anion in dry acetonitrile (260−300 nm). The shoulder band shape was then approximated as the difference between the spectrum in dry acetonitrile and the scaled spectrum of the aqueous solution (Figure 3). This

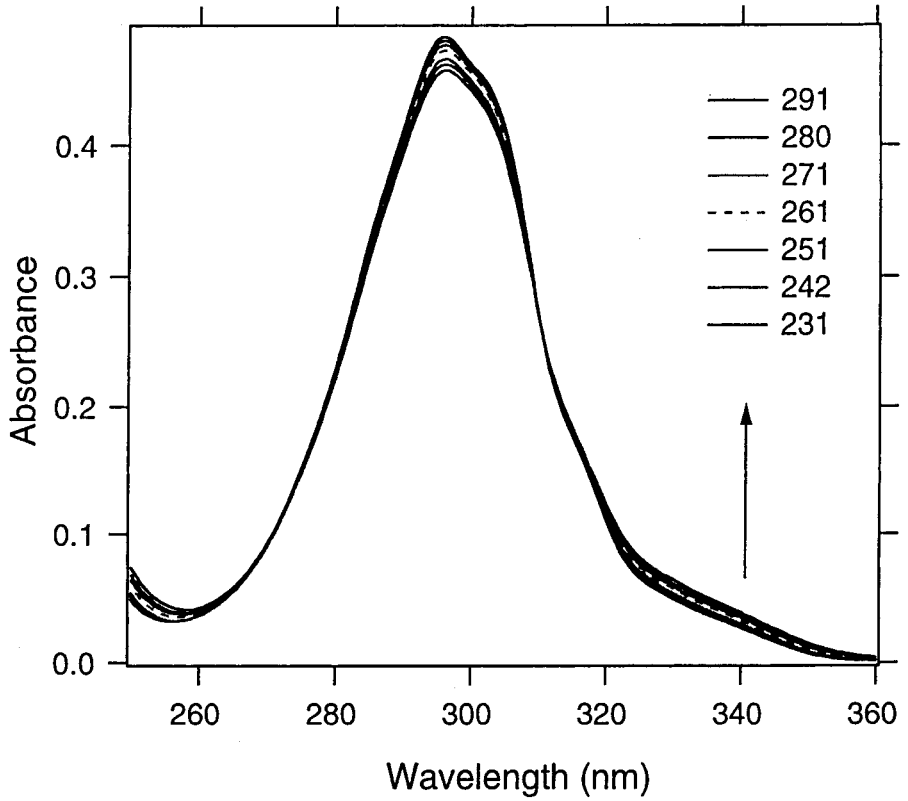

Figure 6. Effect of temperature on the absorption spectrum of sodium salicylate in acetonitrile. The ratio of tautomer to normal absorbance increases with temperature. Note the isosbestic point at 310 nm.

difference band, which peaked at 325 nm, was fit to a Gaussian, which was then incrementally subtracted from the dry acetonitrile spectrum to minimize the shoulder as much as possible without causing a negative deviation on the long-wavelength side of the resulting short-wavelength main band (296 nm). By this method two component spectra, A_N and A_T, were determined for each of the absorption spectra in the temperature range 231−291 K (Figure 6).

The extinction coefficient at the isosbestic point permits calculation of the extinction coefficient for the two component bands. At the isosbestic point (310 nm, Figure 6) the extinction coefficients N and T are equal: $\epsilon_{iso}^{310} = \epsilon_N^{310} = \epsilon_T^{310}$. The slopes of the absorption spectra are relatively steep at the isosbestic point, and therefore the extinction coefficient at the isosbestic point was estimated to be 2000 ± 100 M^{-1} cm^{-1}. Extinction coefficients for the maxima of the major and minor component bands were then calculated by reference to the measured extinction coefficient at the isosbestic point:

$$\epsilon_{N,296} = \epsilon_{iso}^{310}(A_{N,296}/A_{N,310}) = 3586\ M^{-1}\ cm^{-1}$$

$$\epsilon_{T,325} = \epsilon_{iso}^{310}(A_{T,325}/A_{T,310}) = 3400\ M^{-1}\ cm^{-1}$$

The estimated uncertainty in these values is ±100 M^{-1} cm^{-1}. The concentrations of N and T were then calculated from the component absorbances $A_{N,296} = [N]\epsilon_{N,296}l$ and $A_{T,325} = [T]\epsilon^{T,325}l$, where $l = 1$ cm is the sample length. The temperature dependence of K_T is graphed as a van't Hoff plot in Figure 7. The concentration equilibrium constant for [T]/[N] at 298 K was interpolated to be $K_{298} = 0.11$. From the slope and intercept of log(K_T) plotted against $1/T$ (K^{-1}), the enthalpy and entropy difference between the normal and tautomer forms were determined to be $\Delta H = 1.6$ kcal mol^{-1} and $\Delta S = 0.97$ cal·mol^{-1} K^{-1}.

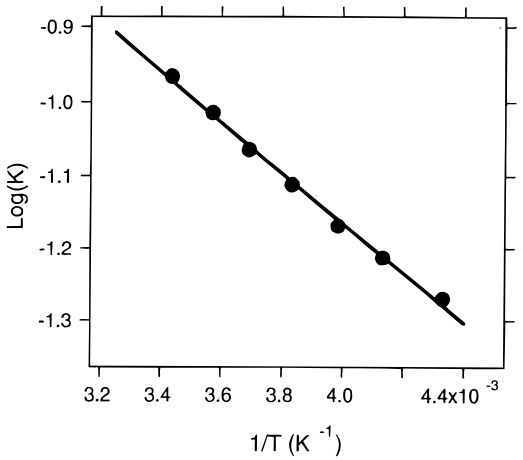

Figure 7. van't Hoff plot of ln(K) vs $1/T$, where K = [T]/[N] as described in the text.

Separation of the absorption into its major and minor component bands (which are assigned in this study to the N and T forms, respectively) also enables an estimate of the fluorescence quantum yield of both forms. First, the fluorescence quantum yield Φ_N for excitation of the normal form of sodium salicylate was estimated as the measured sample quantum yield ϕ_{296} for excitation at 296 nm, using quinine sulfate as the standard, according to $\phi_{296} = \phi_r A_r F_s / A_{s,296} F_r$. The indices r and s refer to the quinine sulfate standard (r) and salicylate sample (s), A refers to the absorbance at the wavelength of excitation, and F is the area under the emission curves of r and s. The fluorescence quantum yield Φ_T for excitation of the tautomer was then estimated as the sample *relative* quantum yield ϕ_{340} for excitation on the long-wavelength side of the absorption band (340 nm) where there is little absorption by the normal form N: $\phi_{340} = \phi_{296}$ ($A_{s,296}F_{s,340}/A_{s,340}F_{s,296}$), where the inte-

grated fluorescence intensities are now also indexed by their respective excitation wavelengths. This analysis is possible because the component absorbances were determined by the absorption band decomposition described above. This estimate of the fluorescence quantum yields assumes that the observed fluorescence arises predominantly, possibly solely, from the tautomer form, as supported by the invariance of fluorescence band shape and lifetime with excitation wavelength (see below). Optically thin samples were used for sample and reference fluorescence quantum yield measurements. The fluorescence quantum yield for excitation in the long-wavelength shoulder (340 nm) is approximately 60% larger than the yield for excitation in the main band at 296 nm ($\phi_{340} = 0.29$, $\phi_{296} = 0.18$) in acetonitrile at room temperature.

The fluorescence lifetime in dry acetonitrile is practically the same for excitation in both the main absorption band (4.85 ns, 282.5 nm excitation) and the long-wavelength shoulder (4.83 ns, 336 nm excitation). The steady-state fluorescence anisotropy excited at 296 nm in ethanol glass at 80 K is constant, 0.30 ± 0.01, across the fluorescence spectrum (380−440 nm). In this glass the excitation polarization spectrum is constant across the absorption band (275−330 nm, monitored at 410 nm). In the low-temperature glass, the excitation intensity of the long-wavelength shoulder band is too weak to distinguish its anisotropy from that of the main band. However, in room-temperature acetonitrile the time-resolved fluorescence anisotropy decay curves show that the initial anisotropy is high for excitation into both the main and shoulder bands (0.32 at 300 nm and 0.33 at 336 nm excitation). This is consistent with the steady-state anisotropy in ethanol glass ($A_{cw} = 0.30$), indicating that the excitation (N* ← N) and emission (T* → T) transition dipole moments are approximately parallel. Although both N and T species are excited at 336 nm, the constancy of the limiting anisotropy implies that the transition moment of the longer wavelength species is parallel to N* ← N excitation, consistent with the assignment of the longer wavelength band to T* ← T excitation. The anisotropy decay curves were fit to a single exponential, with fitted rotational diffusion time constants that are the same within experimental error, 16.7 ps at 300 nm and 16.4 ps at 336 nm excitation characteristic of rotational diffusion of a spherical solute with a mean diameter of 0.7 nm.

The excitation and emission transition moments may be very nearly parallel. In rigid ethanol glass at 80 K, the constancy of the fluorescence anisotropy across the fluorescence band indicates that the T* → T fluorescence transition is electronically allowed and the amount of vibronic mixing is very small. There are several processes that can make the measured anisotropy less than the ideal value of 0.4 for parallel excitation and emission transition moments. First, the excitation transition may be slightly vibronically mixed. If vibronic mixing reduces the fractional excitation probability along the emission axis to 0.9 (i.e., 10% of the excitation intensity is orthogonal to the emission axis), A_0 will be reduced to 0.33. However, a common indication of vibronic mixing in an excitation band is variation (usually a decrease) of anisotropy with decreasing wavelength, as the excitation energy is scanned up from the band origin. However, the constancy of the excitation anisotropy across the absorption spectrum indicates that N → N* is allowed with little vibronic mixing. Thus, within the accuracy of our measurement, the vibronic component of the excitation intensity is probably less than 10%. Intrinsic randomization and instrumental depolarization also reduce measured anisotropy. Practical anisotropy measurements seldom record values near the maximum 0.4, even with careful corrections for instrumental polarization bias with "*g*" factors, largely because of instrumental depolarizing effects, notably large aperture optics, unrecognized strain birefringence (especially serious in low-temperature glassy solvents), and solute rotational diffusion in organic glasses. These effects have been treated quantitatively and reviewed.[72,73] For example, in a practical right-angle photoselection system, it was found that decreasing the collection *f*/number from *f*/6 to *f*/2 reduced measured anisotropy of anthracene (0−1 and 1−0 bands) from 0.37 to 0.34.[68] Thus, the intrinsic salicylate anisotropies are high for excitation into both bands (296 and 325 nm), and all transition moments in the photocycle are very nearly parallel, supporting the interpretation that the electronic states are correlated and dipole allowed (i.e., weak or negligible vibronic mixing).

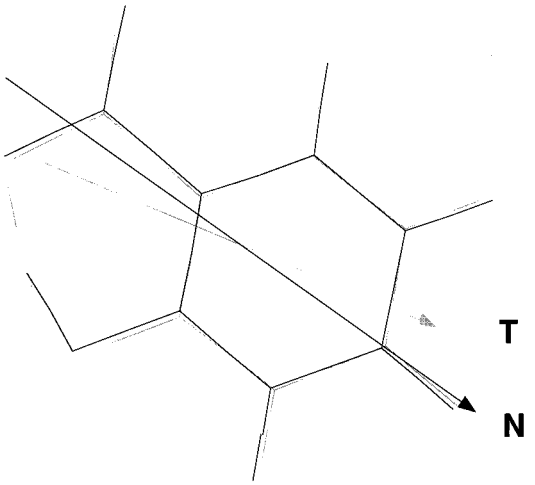

Figure 8. Optimized structures of N and T isomers of salicylate anion with superimposed dipole moments (solid, N; shaded, T): $\mu(N) = 6.9$ D; $\mu(T) = 5.0$ D.

We now discuss the properties of the photocycle structures. Optimized isolated molecule structures were determined for ground-state N and T isomers by an ab initio method, and solvent effects were modeled by the isodensity polarized continuum model (IPCM).[74] Excitation energies, transition moments, and oscillator strengths at the optimized N and T geometries were determined for N* and T* using a semiempirical method parametrized for spectroscopic properties.[75−77] These are described below and discussed in the context of prior qualitative considerations of perturbation effects of inductive substituents on the benzene ring and the role of charge-transfer character inducing ESIPT.

Equilibrium gas-phase geometries and harmonic vibrational frequencies of the N and T ground-state tautomers, as well as the proton-bridging transition state, were calculated at the MP2 level of theory (Møller−Plesset second-order perturbation theory) within the frozen core approximation (the C and O 1s-like electrons were not correlated). The one-particle basis set corresponded to the standard aug-cc-pVDZ basis set of Dunning and co-workers[78,79] with the omission of the diffuse d-type polarization functions on C and O and the diffuse p-type functions on H. The calculated structures and dipole moments of N and T are shown in Figure 8. Transfer of the proton from phenol to the carboxyl group results in shortening of the phenoxide C−O bond and the ring-carboxyl C−C bond with concomitant lengthening of the carboxyl C−OH bond. In addition, the aromatic ring bonds alternatively lengthen and shorten, as shown in Figure 9. These changes are consistent with significantly increased quinoidal character of the tautomer

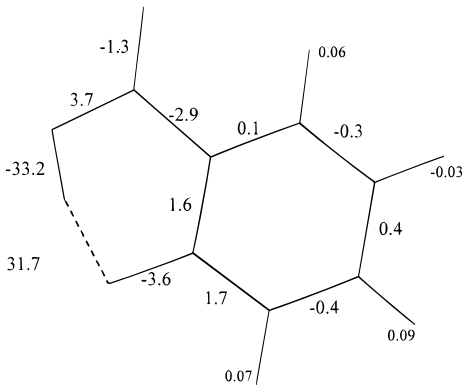

Figure 9. Bond length differences $\Delta = R_N - R_T$ in picometer units for the ab initio structures shown in Figure 8.

T electronic structure (Figure 2). (Optimized coordinates are available on request from the authors.) At this level of theory, the minor tautomer (T) is higher in energy than the major (N) form by 0.17 kcal/mol. The intervening, bridging transition state is located 0.36 kcal/mol above the N tautomer. Harmonic zero-point energy (ZPE) vibrational effects, however, yield a tautomerization energy of just −0.01 kcal/mol; i.e., the major and minor tautomers are isoenergetic in the gas phase. In addition, with the inclusion of ZPE corrections the barrier disappears altogether ($\Delta E_b = -1.32$ kcal/mol).

To estimate the effects of solvation on the relative energetics, the IPCM[74] was employed at the MP2 level of theory with the basis set as described above and the optimized gas-phase geometries. Dielectric constants of 78.54 and 37.5 were used for water and acetonitrile, respectively.[80] In each case, the N tautomer is strongly stabilized relative to the T form. With the use of the larger dielectric constant (water), the N tautomer is stabilized by 3.3 kcal/mol relative to T and the bridged transition-state structure is higher than N by 2.2 kcal/mol. Addition of the gas-phase harmonic ZPE corrections leaves the T tautomer 3.1 kcal/mol above the major form and the bridging structure 0.5 kcal/mol above N. The relative energetics obtained using the acetonitrile dielectric constant were essentially identical. It should be noted that our results are in good agreement with the recent calculations of Shapley et al.,[4] where a similar correlation method and basis set were used.

Because of the low symmetry of salicylate, the Franck−Condon accessible lowest excited singlet state has been considered to be correlated with both the ^1L_a and ^1L_b states of substituted benzene compounds. In a comparative study of the systematics in the electronic spectra of polar ortho, meta, and para disubstituted benzene derivatives, McGlynn et al. showed that ortho substitution on benzene by a moderate-strength electronic donor (−OH) and acceptor (−CO_2R) always resulted in the ^1L_b lowest excited singlet state.[57,58] Because vibronic coupling in ^1L_b states is much weaker than in ^1L_a states, the electronic allowed character of the transition will dominate the anisotropy of the excitation and emission, resulting in relatively constant anisotropy across the fluorescence and excitation spectra. This constancy of anisotropy is displayed by salicylate anion. It has recently been argued by Nagaoka[28,29] that the electronic potential gradients leading to proton transfer require a nodal plane in the electronic wave function between the ortho electron donor (−OH) and acceptor (−CHO or CO_2R). This electronic configuration would result in a transition dipole moment directed parallel to the aromatic bond connecting the donor and acceptor. In para disubstituted benzenes of C_{2v} symmetry, the ^1L_a transition carries significant charge transfer and also lies parallel to the symmetry axis and perpendicular to an electronic nodal plane that cuts across the aromatic bonds. Nagaoka correlates the lowest excited state of ortho disubstituted benzenes, such as *o*-hydroxybenzaldehyde, with the ^1L_a state.[25−30]

Inductive perturbations by the donor and acceptor groups result in substituent specific transition moment parameters that have opposite sign.[81−83] Applying the rules of Petruska and Platt to the benzene $^1B_{2u}$ wave function (^1L_b) using the transition moments induced by each substituent,[84,85] it is seen that ortho hydroxyl and carboxylate substitution on benzene results in an induced transition dipole moment for the ^1L_b state that is *parallel* to the transition dipole moment computed by Nagaoka et al.,[28,29] i.e., a transition with the appearance of ^1L_a (i.e., atom-to-atom) that derives from inductive perturbation of the benzene $^1B_{2u}$ (^1L_b) state. It is not the low symmetry per se of the ortho donor−acceptor substitution that creates this apparent rotation of the ^1L_b transition moment from bond-to-bond toward the atom-to-atom direction. Instead, the direction is established by the combined action of the alternating sign of the ^1L_b wave function at adjacent, ortho carbon atoms and the opposite signs of the inductive spectroscopic moments of the donor (hydroxyl) and acceptor (carboxyl) groups. These qualitative concepts on the effects of inductive substituents (^1L_b) and the direction of charge transfer between donor and acceptor (^1L_a) both predict an atom-to-atom transition moment parallel to the aromatic bond connecting the substituents, but they disagree on the state assignment.

The assignment of normal and ESIPT salicylate excited states (^1L_a or ^1L_b) can be settled by recognizing that the transition density patterns, not the location of nodes or the transition moment directions, determine the assignment.[75,76] Semiempirical INDO/S-CIS quantum chemical computations[77] (ZINDO) using 196 singly excited configurations, Mataga−Nishimoto electron repulsion integrals, and the original overlap factors[77] were performed on the ground-state N and T optimized geometries obtained from the ab initio calculations described above. Transition densities computed for the lowest five $^1\pi\pi^*$ states, using the ground-state N and T ab initio optimized geometries, are shown in Figure 10 (normal) and Figure 11 (tautomer), together with transition moments, oscillator strengths, and wavelengths. The transition densities support an assignment of ^1L_b to the lowest singlet$^1\pi\pi^*$ state on both N* (294 nm) and T* (329 nm). The resulting transition densities are clearly centered on the bonds in N → N*, and T → T* is similar but slightly admixed with ^1L_a, with some transition density appearing on the phenyl carbon connected to the carboxyl group. The ^1L_b transition moments of N* and T* are computed to be nearly parallel and are directed nearly bond-to-bond, i.e., with respect to the phenyl−carboxyl bond, μ_{NN^*} is 35° and μ_{TT^*} is 41°. These angles are 20−25° closer to the carboxyl group than the atom-to-atom transition direction predicted by the qualitative concepts discussed above. The transition moments are not parallel to the aromatic bond connecting the donor and acceptor group. The ratio of computed oscillator strengths $f_N/f_T = 0.39$ is smaller than the experimentally estimated ratio of extinction coefficients $\epsilon_N/\epsilon_T = 1.06$. The reason for this discrepancy is not known.

The ab initio calculation gives permanent dipole moments of μ(T) = 5.0 D < μ(bridged) = 5.8 D < μ(N)= 6.9 D, where the bridged geometry places the proton on the small energy barrier between N and T geometries. The semiempirical static dipole moments of the excited states N* and T* do not appear to be much larger than their respective ground-state dipole moments ($\Delta\mu_{NN^*}$= 0.148 D; $\Delta\mu_{TT^*}$ = 1.03 D). This is characteristic of ^1L_b states, which are known to possess little

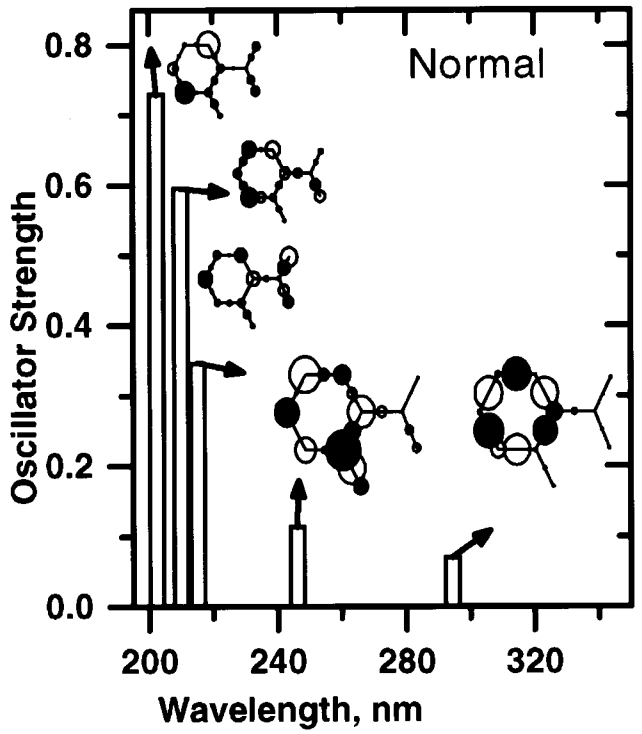

Figure 10. Transition moments and transition densities computed by the ZINDO method for the normal form. Arrows indicate transition moment directions relative to the phenyl-to-carboxyl bond (horizontal).

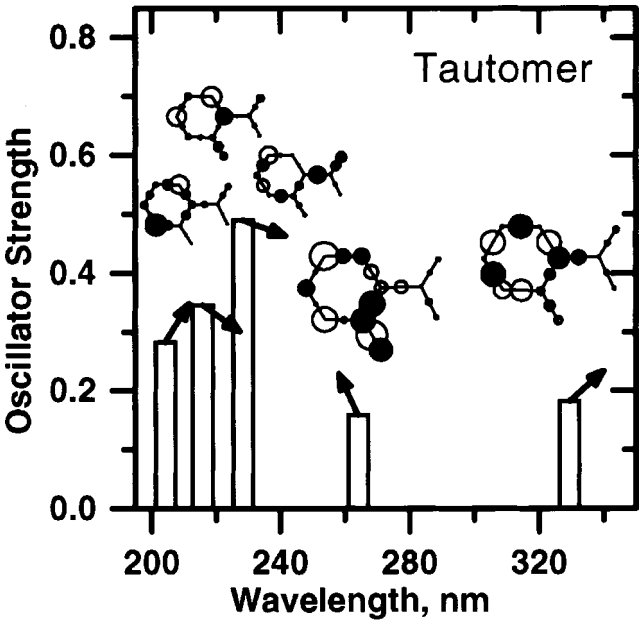

Figure 11. Transition moments and transition densities computed by the ZINDO method for the tautomer form. Arrows indicate transition moment directions relative to the phenyl-to-carboxyl bond (horizontal).

charge-transfer character and may be contrasted with the frequently large charge-transfer character of ^1L_a states. The slightly increased ^1L_a character of the T* state is also consistent with a larger $\Delta\mu_{TT^*}$. These calculations are consistent with the observed absorption/excitation spectrum which red shifts very slightly with increasing solvent polarity (e.g., see Figure 4). The solvent polarity dependence of the fluorescence maximum is more complicated, showing a definite red shift with increasing polarity of protic solvents (alcohols and water), but showing a slight but distinct blue shift with increasing polarity of nonprotic solvents. This behavior suggests that specific solvent−solute interaction may influence the excited-state charge distribution and dipole moments. The semiempirical calculations also suggest that N* is more polar than T*, which is reasonable if the proton transfer is a response to increased electric field gradients in the excited state (μ(N*) − μ(T*) = 1.2 D). Therefore, we conclude μ(N*) ≥ μ(N) > μ(T*) > μ(T), although these relationships may depend on specific interaction of solute and solvent molecules. Comparing the density differences of the lowest $^1\pi\pi^*$ state, there is some loss of electron density from the phenol oxygen upon excitation of the normal form N, and this is increased upon tautomerization. The dipole moment changes are not large partly because of a large loss of density on the carbon para to the hydoxyl, with density transferred to the meta positions. This charge redistribution tends to cancel the dipole change caused by transfer from the phenol oxygen and also indicates a large quadrupole change. This qualitative description suggests the need for accurate experimental and computational determination of the excited-state dipole moments μ(N*) and μ(T*).

Conclusion

Although many compounds have been shown to exhibit ESIPT, in only a small set of these have both proton tautomers (N and T) been observed in ground-state equilibrium directly by UV−vis absorption or excitation spectra. Most ESIPT molecules studied to date have been neutral and were studied in nonaqueous solutions or in molecular jets as isolated monomers, dimers, or clusters. In protic solvents it is common that intermolecular H-bonding decreases the ratio of ESIPT to normal emission. The salicylate anion is an unusual member of the ESIPT compounds because it is negatively charged and does not show dual fluorescence. Fluorescence from salicylate anion is from the ESIPT state only and is not inhibited by H-bonding to water or other protic solvents. However, protonation to the neutral salicylic acid form severely reduces the fluorescence quantum yield. This unusual behavior is attributed to a strong intramolecular H-bond between the phenolic proton and the negatively charged carboxylate group. It is known that interference of the intramolecular H-bond by inner-sphere complexation of the carboxylate group (e.g., with Al^{3+}) will blue shift the emission, presumably because the fluorescence of the complex arises mainly from the excited normal tautomer form (N*), rather than the ESIPT state (T*).[62] In this paper the long-wavelength shoulder of the UV absorption spectrum of salicylate is assigned to absorption by the ground-state proton-transferred tautomer (T → T*). Alternative assignments to absorption by the dimer, the dianion (deprotonated form), or salicylic acid (protonated form) were eliminated by experimental tests. A common isosbestic point is observed as a function of both temperature and water concentration and is strong evidence for assignment of the long-wavelength shoulder to an isomeric species of the salicylate anion. Protic solvents stabilize the normal form relative to the tautomer form to such an extent that the shoulder band is hardly observable in aqueous solutions. Optimized ground-state structures of the normal and tautomer forms were calculated by ab initio methods for both gas-phase and high dielectric environments. UV absorption energies and transition dipoles calculated at the N and T geometries are consistent with the observed spectra and emission anisotropies. The calculations are consistent with assignment of the near UV shoulder band to T → T* absorption and support the hypothesis that the T and T* electronic structures possess considerably more quinoidal character than the N isomer.

Acknowledgment. We thank Dr. Gary R. Holtom for use of the TCSPC apparatus and Professor Bruce Hudson for stimulating discussions. This research was supported by the Molecular Science Research Initiative at Pacific Northwest National Laboratory and the Chemical Sciences Division in the Office of Basic Energy Sciences of the U.S. Department of Energy. Pacific Northwest National Laboratory is operated for the U.S. Department of Energy by Battelle under Contract DE-AC06-76RLO 1830.

References and Notes

(1) Barbara, P. F.; Patrick, K.; Walsh, L. E.; Brus. *J. Phys. Chem.* **1989**, *93*, 29.

(2) Formosinho, S. J.; Arnaut, L. G. *J. Photochem. Photobiol. A* **1993**, *75*, 21.

(3) There is no uniformly accepted system of naming the four structures of the salicylate photocycle. The recent series of papers (cited below) by Bisht et al. consistently denote N and N* as "enol" and the tautomeric T and T* as "keto", emphasizing the resonance bonding structure of the phenyl−hydroxyl bond (enol in the ground-state N form and keto in the quinoidal T* form). The enol/keto notation may help to identify the dominant resonance structures of N and T* in the neutral acid and esters. However, for the salicylate *anion* this nomenclature can be confusing when the electronic resonance structures of N* and T are discussed. Therefore, in this paper we choose to use a more generic nomenclature (normal N and tautomer T) that avoids structural implications which may have limited generality.

(4) Shapley, W. A.; Bacskay, G. P.; Warr, G. G. *J. Phys. Chem.* **1998**, *A102*, 1938.

(5) Catalan, J.; Palomar, J.; De Paz, J. L. G. *Chem. Phys.* **1997**, *269*, 151.

(6) Bureiko, S. F.; Oktiabr'sky, V. P. *J. Mol. Struct.* **1995**, *349*, 53.

(7) Vener, M. V., Scheiner, S. *J. Phys. Chem.* **1995**, *99*, 642.

(8) Douhal, A.; Sastre, R. *Chem. Phys.* **1994**, *219*, 76.

(9) Parchment, O. G., Burton, N. A.; Hillier, I. H. *Chem. Phys.* **1993**, *203*, 46.

(10) Lavin, A.; Collins, S. *Chem. Phys.* **1993**, *204*, 96.

(11) Lavin, A.; Collins, S. *Chem. Phys.* **1993**, *207*, 513.

(12) Zuccarello, F.; Buemi, G. *Gazz. Chim. Ital.* **1988**, *118*, 359.

(13) Costela, A.; Garcia-Moreno, I. *Chem. Phys.* **1996**, *249*, 373.

(14) Costela, A.; Muñoz, J. M.; Douhal, A.; Figuera, J. M.; Acuña, A. U. *Appl. Phys.* **1989**, *B49*, 545.

(15) Bisht, P. B.; Okamoto, M.; Hirayama, S. *J. Phys. Chem.* **1997**, *101*, 8850.

(16) Bisht, P. B.; Petek, H.; Yoshihara, K.; Nagashima, U. *J. Chem. Phys.* **1995**, *103*, 5290.

(17) Weller, A. *Z. Elektrochem.* **1956**, *60*, 1144.

(18) Helmbrook, L.; Kenny, J. E.; Kohler, B. E.; Scott, G. W. *J. Phys. Chem.* **1983**, *87*, 280.

(19) Law, K.-Y.; Shoham, J. *J. Phys. Chem.* **1994**, *98*, 3114.

(20) Law, K.-Y.; Shoham, J. *J. Phys. Chem.* **1995**, *99*, 12103.

(21) Morgan, M. A.; Orton, E.; Pimentel, G. C. *J. Phys. Chem.* **1990**, *94*, 7927.

(22) Orton, E.; Morgan, M. A.; Pimentel, G. A. *J. Phys. Chem.* **1990**, *94*, 7936.

(23) Herek, J. L.; Pederen, S.; Bañares, L.; Zewail, A. H. *J. Chem. Phys.* **1992**, *97*, 9046.

(24) Goodman, J.; Brus, L. E. *J. Am. Chem. Soc.* **1978**, *100*, 7472.

(25) Nagaoka, S.; Nagashima, U. *Chem. Phys.* **1989**, *136*, 153.

(26) Nagaoka, S.; Hirota, N.; Sumitani, M.; Yoshihara, K.; Lipczynska-Kochany, E.; Iwamura, H. *J. Am. Chem. Soc.* **1984**, *106*, 6913.

(27) Nagaoka, S.; Nagashima, U.; Ohta, N.; Fujita, M.; Takemura, T. *J. Phys. Chem.* **1988**, *92*, 166.

(28) Nagaoka, S.; Nagashima, U. *J. Phys. Chem.* **1991**, *95*, 4006.

(29) Nagaoka, S.; Nagashima, U. *J. Phys. Chem.* **1990**, *94*, 1425.

(30) Nagashima, U.; Nagaoka, S.; Katsumata, S. *J. Phys. Chem.* **1991**, *95*, 5, 3532.

(31) Nagy, P. I.; Dunn, W. J., III; Alagona, G.; Ghio, C. *J. Phys. Chem.* **1993**, *97*, 28.

(32) Nagy, P. I.; Bitar, J. E.; Smith, D. A. *J. Comput. Chem.* **1994**, *15*, 1228.

(33) Nagy, P. I.; Smith, D. A.; Alagona, G.; Ghio, C. *J. Phys. Chem.* **1994**, *98*, 486.

(34) Kosower, E. M.; Huppert, D. *Ann. Phys. Chem.* **1986**, *127*.

(35) Orttung, W. H.; Scott, Gary W.; Vosooghi, D. *THEOCHEM* **1984**, *18*, 161.

(36) Joshi, H. C.; Mishra, H.; Tripathi, H. B. *Am. Chem.* **1997**, *105*, 15.

(37) Huppert, D.; Gutman, M.; Kaufmann, K. J. *Adv. Chem. Phys.* **1981**, *XLVII*, 643.

(38) Feng, J.; Teng, Q.; Xu, W.; Li, Z.; Sun, C. *Gaodeng Xuexiao Huaxue Xuebao* **1993**, *14*, 527.

(39) Sanchez-Cabezudo, M.; De Paz, J. L. G.; Catalan, J.; Amat-Guerri, F. *J. Mol. Struct.* **1985**, *131*, 277.

(40) Lahmani, F.; Zehnacker-Rentien, A. *J. Phys. Chem. A* **1997**, *101*, 6141.

(41) Douhal, A.; Amat-Guerri, F.; Acuña, A. U. *J. Phys. Chem.* **1995**, *99*, 9, 91.

(42) Gormin, D.; Kasha, M. *Chem. Phys.* **1988**, *153*, 574.

(43) Heldt, J.; Gormin, D.; Kasha, M. *Chem. Phys.* **1989**, *136*, 321.

(44) Swinney, T. C.; Kelley, D. F. *J. Phys. Chem.* **1991**, *95*, 10369.

(45) Swinney, T. C.; Kelley, D. F. *J. Chem. Phys.* **1993**, *99*, 211.

(46) Brucker, G. A.; Swinney, T. C.; Kelley, D. F. *J. Phys. Chem.* **1991**, *95*, 3190.

(47) Dzugan, T. P.; Schmidt, J.; Aartsma, T. J. *Chem. Phys.* **1986**, *127*, 336.

(48) Estevez, C. M.; Rios, M. A.; Rodriguez, J. *Struct. Chem.* **1992**, *3*, 381.

(49) Yuzawa, T.; Takahashi, H.; Hamaguchi, H. *Chem. Phys.* **1993**, *202*, 221.

(50) Parthenopoulos, D. A.; McMorrow, D. P.; Kasha, M. *J. Phys. Chem.* **1991**, *95*, 2668.

(51) Acuna, A. U.; Amat, F.; Catalan, J.; Costela, A.; Figuera, J. M.; Munoz, J. M. *Chem. Phys.* **1986**, *132*, 567.

(52) Meyer, J. A.; Itzkan, I.; Kierstead, E. *Nature* **1970**, *225*, 544.

(53) Catalan, J.; Fernandez-Alonso, J. I. *J. Mol. Struct.* **1975**, *27*, 59.

(54) Sundaralingam, M.; Jensen, L. H. *Acta Crystallogr.* **1965**, *18*, 1053.

(55) Lin-Vien, D.; Colthup, N. B.; Fateley, W. G.; Grasselli, J. G. *The Handbook of Infrared and Raman Characteristic Frequencies of Organic Molecules*; Academic Press: San Diego, 1991.

(56) Yost, E. C.; Tejedor-Tejedor, M. I.; Anderson, M. A. In situ CIR−FTIR characterization of salicylate complexes at the goethite/aqueous solution interface. *Environ. Sci. Technol.* **1990**, *24*, 822−828.

(57) Carsey, T. P.; Findley, G. L.; McGlynn, S. P. *J. Am. Chem. Soc.* **1979**, *101*, 4502.

(58) Findley, G. L.; Carsey, T. P.; McGlynn, S. P. *J. Am. Chem. Soc.* **1979**, *101*, 4511.

(59) Berlman, I. B. *Handbook of Fluorescence Spectra of Aromatic Molecules*, 2nd ed.; Academic Press: New York, 1997; Graph 34A, p 166 and discussion pp 27−28.

(60) The formal definition of Stokes *loss* is not appropriate in discussing salicylate spectra because the definition assumes a common electronic origin for excitation and emission and does not account for excited-state isomerizations (such as tautomerization). We refer to the Stokes *gap* as the experimental difference between the maxima of excitation and emission bands. The fluorescence is described qualitatively as Stokes *shifted*. This common usage is unambiguous and represents qualitatively the combined energy loss of all processes including vibrational relaxation, functional group rotation, and tautomerization.

(61) Weller, A. *Prog. React. Kinet.* **1961**, *1*, 188.

(62) Ainsworth, C. C.; Friedrich, D. M.; Gassman, P. L.; Wang, Z.; Joly, A. G. *Geochim. Cosmochim. Acta* **1998**, *62*, 595.

(63) Tuin, G.; Candau, F.; Zana, R. *Colloids Surf., A* **1998**, *131*, 303.

(64) Butner, C. L.; Viehmann, W. *Appl. Opt.* **1984**, *23*, 2046.

(65) Masuda, F. *Sci. Light (Tokyo)* **1965**, *14*, 147.

(66) Holtom, G. R. *Time-Resolved Laser Spectrosc. Biochem., SPIE* **1990**, *1204*, 2.

(67) Albrecht, A. C. *J. Mol. Spectrosc.* **1961**, *6*, 84.

(68) Friedrich, D. M. *Ph.D. Dissertation*, Cornell University, University Microfilms, 1973.

(69) Lakowicz, J. R. *Principles of Fluorescence Spectroscopy*; Plenum Press: New York, 1983; Vol. 5, p 111.

(70) Kliger, D. S.; Lewis, J. W.; Randall, C. E. *Polarized Light in Optics and Spectroscopy*; Academic Press: New York, 1990; p 304.

(71) Steiner, R. F. In Fluorescence anisotropy: theory and application. *Topics in Fluorescence Spectroscopy 2. Principles*; Lakowicz, J. R., Ed.; Plenum Press: New York, 1991; pp 1−52.

(72) Turrell, G. *J. Raman Spectrosc.* **1984**, *15*, 8.

(73) Bremard, C.; Laureyns, J.; Turrell, G. *Can. J. Spectrosc.* **1987**, *32*, 70.

(74) Frisch, M. J.; Trucks, G. W.; Schlegel, H. B.; Gill, P. M. W.; Johnson, B. G.; Robb, M. A.; Cheeseman, J. R.; Keith, T.; Petersson, G. A.; Montgomery, J. A.; Raghavachari, K.; Al-Laham, M. A.; Zakrzewski, V. G.; Ortiz, J. V.; Foresman, J. B.; Cioslowski, J.; Stefanov, B. B.; Nanayakkara, A.; Challacombe, M.; Peng, C. Y.; Ayala, P. Y.; Chen, W.; Wong, M. W.; Andres, J. L.; Replogle, E. S.; Gomperts, R.; Martin, R. L.; Fox, D. J.; Binkley, J. S.; Defrees, D. J.; Baker, J.; Stewart, J. P.; Head-Gordon, M.; Gonzalez, C.; Pople, J. A. *Gaussian 94*, Revision D.1; Gaussian, Inc.: Pittsburgh, PA, 1995.

(75) Callis, P. R. *Int. J. Quantum Chem.: Quantum Chem. Symp.* **1984**, *18*, 579.

(76) Callis, P. R. *J. Chem. Phys.* **1991**, *95*, 4230.

(77) Ridley, J.; Zerner, M. *Theor. Chim. Acta (Berlin)* **1973**, *32*, 111.

(78) Dunning, T. H., Jr. *J. Chem. Phys.* **1989**, *90*, 1007.
(79) Kendall, R. A.; Dunning, T. H., Jr.; Harrison, R. J. *Chem. Phys.* **1992**, *96*, 6796.
(80) Lide, D. R., Ed.; *CRC Handbook of Chemistry and Physics*, 72nd ed.; CRC Press: Boca Raton, FL, 1991−1992; p 8.51.
(81) Petruska, J. *J. Chem. Phys.* **1961**, *34*, 1111.
(82) Petruska, J. *J. Chem. Phys.* **1961**, *34*, 1120.
(83) Platt, J. R. *J. Chem. Phys.* **1951**, *19*, 271.
(84) Stevenson, P. E. Effects of Strongly Perturbing Substituents on the Electronic Spectra of Benzene. Ph.D. Thesis, Part 1, Department of Chemistry, University of Chicago, 1964.
(85) Stevenson, P. E. *J. Chem. Educ.* **1964**, *41*, 234.